Exchange of TiO_2 Nanoparticles between Streams and Streambeds

NATALIA TICIANA BONCAGNI,[†] JUSTO MANUEL OTAEGUI,[†] EVELYN WARNER,[†] TRISHA CURRAN,[‡] JIANHONG REN,*[,‡] AND MARIA MARTA FIDALGO DE CORTALEZZI[†]

Department of Chemical Engineering, Instituto Tecnologico de Buenos Aires, Av. Eduardo Madero 399, 1106 Buenos Aires, Argentina, and Department of Environmental Engineering, Texas A&M University-Kingsville, Kingsville, Texas 78363

Received February 12, 2009. Revised manuscript received August 21, 2009. Accepted August 27, 2009.

The expanding use of manufactured nanoparticles has increased the potential for their release into the natural environment. Particularly, TiO_2 nanoparticles pose significant exposure risk to humans and other living species due to their extensive use in a wide range of fields. To better understand the environmental and health risks associated with the release of TiO_2 nanoparticles, knowledge on their fate and transport is needed. This study evaluates the transport of two different TiO_2 nanoparticles: one commercially available (P25 TiO_2) and the other synthesized at a lab scale (synthesized TiO_2). Laboratory flume, column, and batch experiments were conducted to investigate the processes dominating the transport of TiO_2 nanoparticles between streams and streambeds and to characterize the properties of these nanoparticles under different physicochemical conditions. Results show that the synthesized TiO_2 was more stable compared to the P25 TiO_2, which underwent significant aggregation under the same experimental conditions. As a result, P25 TiO_2 deposited at a faster rate than the synthesized TiO_2 in the streambed. Both types of TiO_2 nanoparticles deposited in the streambed were easily released when the stream velocity was increased. The aggregation and deposition of P25 TiO_2 were highly dependent on pH. A process-based colloid exchange model was applied to interpret the observed transport behavior of the TiO_2 nanoparticles.

Introduction

The expanding use of nanomaterials has increased the potential for their release into the natural environment. Particularly, TiO_2 nanoparticles (NPs) pose significant exposure risk to humans and other living species due to their extensive use as pigment, photocatalyst, absorbent, and catalytic support and in sunscreens, cosmetics, and wastewater treatment (*1*). The environmental significance of NPs generally derives from their small sizes, high surface areas, and novel chemistry, which are easily altered under different environmental conditions (*2*–*5*). This increased surface reactivity predicts that NPs exhibit greater biological activity per given mass and very different fate and transport behaviors compared with larger particles of the same materials, which raises uncertainties on the applicability of current models, most of which do not account for aggregation, a common phenomenon with NPs (*4, 6, 7*). To better understand the environmental impacts and health risks associated with the release of TiO_2 nanoparticles, we need more knowledge on their fate and transport and the applicability of available transport models.

Stream–subsurface exchange is the exchange of solute between surface water and the shallow subsurface generally occurring in streams and is induced by the streambed topography such as sand waves or pools and riffles (*8, 9*). This exchange process can carry small particles into streambeds, where extensive particle retention can occur due to their increased contact with streambed sediments and subsequent processes such as filtration and straining (*10*–*12*). As a result, bed sediments and pore water can become a significant reservoir of pollutants and a source of contamination long after the original pollutant input ceases (*13, 14*). Stream–subsurface exchange plays a key role in the transport of particles, contaminants, and ecologically relevant substances in streams as demonstrated by many previous studies (e.g., *10*–*12, 15*).

Substantial work on the fundamental understanding of stream–subsurface exchange processes has been conducted (e.g., *8, 10*–*12, 16*–*18*). A process-based colloid exchange model was developed by Packman et al. (*11, 12*). The physicochemical processes considered in this model include colloid filtration and settling in addition to stream–subsurface hydraulic exchange (*11*). This model has been examined in detail using laboratory experiments and was successfully applied to describe the exchange of submicrometer- and micrometer-sized particles (*10*–*12, 15*). The purpose of this study was to demonstrate the extent of the stream–subsurface exchange of TiO_2 NPs and examine the applicability of the colloid exchange model of Packman et al. (*11*) in describing the transport of NPs.

Materials and Methods

Recirculating Flume. The exchange experiments were conducted in a recirculating flume to simulate a sand bed stream in a laboratory setting. This type of flume system has been extensively used in laboratory studies of stream–subsurface exchange due to its easy control of physicochemical conditions (*10*–*12*). The flume has a test section of 350 cm length, 20 cm width, and 50 cm depth (see Figure S1-A,Supporting Information (SI)). Water and sediments can both be returned to the upstream end of the channel via a pump and a return pipe. A nylon mesh was used to retain the bed sediments at the downstream end of the channel.

Bed Sediments. Ottawa No. 12 Flint silica sand (U.S. Silica Company, Berkeley Springs, WV) was used as model bed sediment. This sand is commonly used in laboratory experiments because of its high purity (99.8% SiO_2). Sieve analysis indicated that it had a narrow size distribution with $d_{50} = 529$ μm by mass, a geometric mean $d_g = 524$ μm by mass, and a geometric standard deviation $\sigma_g = 1.2$ (dimensionless) (*10*). The sand has a hydraulic conductivity of 10.71 cm/min and a porosity of 0.36. It was cleaned first with deionized (DI) water, followed by weak acid (pH $\sim$ 3.0) and basic (pH $\sim$ 10.5) solution washes (*12*).

Nanoparticles. To investigate the possibly different transport behaviors of different forms of TiO_2, two types of TiO_2 NPs were used. The synthesized TiO_2 suspension was manufactured through a simple and well-studied acidic (pH 3–3.5) peptization process (*19*) at Universidad de Buenos

* Corresponding author phone: 361-593-2798; fax: 361-593-2069; e-mail: jianhong.ren@tamuk.edu.
[†] Instituto Tecnologico de Buenos Aires.
[‡] Texas A&M University-Kingsville.

TABLE 1. Experimental Conditions for Flume Experiments and Parameters Estimated for Exchange Model Application

	run number						
	1A[a]	1B	2A[a]		2B	3A	3B	4A
stream depth, cm	10.13	9.32	10.58		8.96	9.88	9.11	10.82
stream velocity, cm/s	16.14	15.45	15.33		18.23	18.06	15.75	13.23
bed depth (d_b), cm	9.98	10.88	9.60		11.08	10.55	10.79	9.22
bedform height, cm	2.27	1.23	2.94		2.22	2.15	1.13	1.67
λ, cm[b]	20.3	22.7	20.2		21.5	20.2	22.5	15.6
u_m, cm/min[c]	0.106	0.070	0.104		0.132	0.131	0.073	0.080
h_m, cm[d]	0.03	0.02	0.03		0.04	0.04	0.02	0.02
NP, mg/L	8.4[e]	5.9[e]	30[f]		34[f]	30[f]	32[f]	28[f]
pH	6.4	5.9	6.0		6.0	10.0	10.0	6.0
filtration and NP settling parameters								
d_p, μm[g]	0.09	–	0.27	2.80	10.0	–	0.27	–	–
α_c[h]	0.043	–	2.154	0.407	0.035	–	0.033	–	–
η[i]	0.090	–	0.036	0.421	5.163	–	0.036	–	–
λ_f[j] cm^{-1}	0.073	–	1.482	3.292	3.434	–	0.023	–	–
v_s, cm/min[k]	0.0	–	0.0	0.073	0.929	–	0.0	–	–

[a] Runs with multiple phases. The pH was raised to 11.3 in phase II and the flow rate was doubled in phase III. [b] Bedform wavelength. [c] The maximum Darcy velocity. It is the approach (superficial) velocity used in the TE equation. [d] Half amplitude of the head variation over the bedform. [e] Synthesized TiO_2. [f] P25 TiO_2. [g] Estimated from Figures 1 and 2. [h] Estimated from column experiments (see Table S1, SI). [i] Calculated from the TE equation. [j] Calculated using eq 3 and used in simulations for flume results. [k] Calculated using Stokes law and used in simulations for flume results.

Aires Inorganic Chemistry Laboratory (UBAICL), Facultad de Ciencias Exactas y Naturales, Buenos Aires, Argentina (see detailed procedure provided in Text S1, SI). The Aeroxide P25 was provided by the manufacturer (Evonik Degussa Corporation, Parsippany, NJ). It is a hydrophilic fumed TiO_2, a mixture of the rutile and anatase forms with an average primary particle size of 21 nm.

Flume Experiments. All flume experiments (Table 1) were carried out using 0.9 mM NaCl (Mallinckrodt Baker, Inc., Phillipsburg, NJ, with a purity of 99−100%) to characterize the hydraulic exchange process and provide a desired background ionic strength. The flow rate was kept at 3.2 L/s to maintain stationary bedforms and a turbulent flow in the stream. The bedform dimensions and depths of streambed and streamwater were chosen to be comparable with previously published results (*10, 15*). Low initial in-stream particle concentrations were used in flume runs 1A and 1B due to the limited amount of synthesized TiO_2 NP available and some mass loss that occurred after particles were injected in the flume end well. However, this difference in initial particle concentration was not expected to affect the results presented in this paper due to the absence of aggregation for the synthesized TiO_2 under the experimental conditions tested.

In runs 1A and 2A, the pH was raised to 11.3 at the end of the exchange experiment, following which the flow rate was increased to twice the initial flow rate. This was to test the possible release of previously deposited TiO_2 NPs from the sand bed under high pH or high shear conditions. Flume runs 1B−3B were conducted to test the reproducibility of the results obtained in runs 1A−3A, respectively. Given the known photocatalytic activity of the TiO_2 NPs, run 4A was conducted with the entire flume channel being covered using heavy duty aluminum foil to determine if the presence of light contributed to the P25 TiO_2 transport behavior observed in runs 2A and 2B. DI water was used in all experiments, with NaOH (certified ACS grade from Fisher Scientific, Fair Lawn, NJ) added to obtain desired high pH conditions. The flume was operated with a 0% channel slope in all experiments. No significant dissolution of the test NPs was expected under the experimental conditions used (*20−22*).

The flume experiments were started after stationary dune shape bedforms were developed and a uniform flow condition was reached (usually a minimum of 24 h is required). The depth of the stream and streambed, stream velocity, and bedform geometry were measured. Before each flume injection, the desired chemical (pH and ionic strength) conditions were established. The flume experiments consisted of two separate phases. During the first phase, 0.9 mM NaCl was poured slowly into the downstream end well over one recirculating period. The NaCl concentrations in the streamwater were determined by measuring the solution specific conductance using a Horiba ES-12 conductivity meter over time. When the pore water and the recirculating water reached the same sodium concentration, the second phase was initiated by injecting desired amount of TiO_2 NPs following the same injection procedure as used in the first phase. The change in TiO_2 concentration was monitored over time for 48−72 h.

Characterization of Nanoparticles. The size and shape of NP dry powders were examined using scanning electron microscopy (SEM) (Phillips XL30 TMP, FEI/Phillips Inc., Hillsboro, OR) and transmission electron microscopy (TEM) (Phillips EM301, Veeco FEI Inc., Hillsboro, OR). The phase structure of the NPs was investigated using Ultima IV multipurpose X-ray powder diffraction with Copper (Cu) diffractometer and visual XRD Jade 7 software (Rigaku Americas Incorporation, Houston, TX). The NP hydrodynamic size (the size of aqueous phase NPs) was measured using a Malvern Nanosizer ZS (Malvern Instruments, UK). The aqueous phase NP zeta potential was measured using a BIC ZetaPALS (Brookhaven Instruments Corporation, New York). The Nanosizer ZS uses dynamic light scattering (DLS) technique to measure the hydrodynamic size of NPs, which is a function of NP properties such as size and surface structures and solution chemistry such as concentration and type of ions in the medium (*27*).

The absorbance of NPs was measured using an UV−vis Aquamate spectrophotometer and UV−vis 1650 PC (Shimatzu Corporation, Japan) at wavelengths of 327 nm for P25 TiO_2 and 230 nm for the synthesized TiO_2. The detection limit of the technique was <0.1 mg/L for the TiO_2 particles tested. Linear calibration curves were developed for each type of NPs at the working concentrations. To test the potential measurement errors due to aggregation, three calibration curves were developed for P25 TiO_2 after stirring for 0, 4, and 72 h. For the results obtained from flume run 2A, less than 6.5% error was obtained for the dimensionless

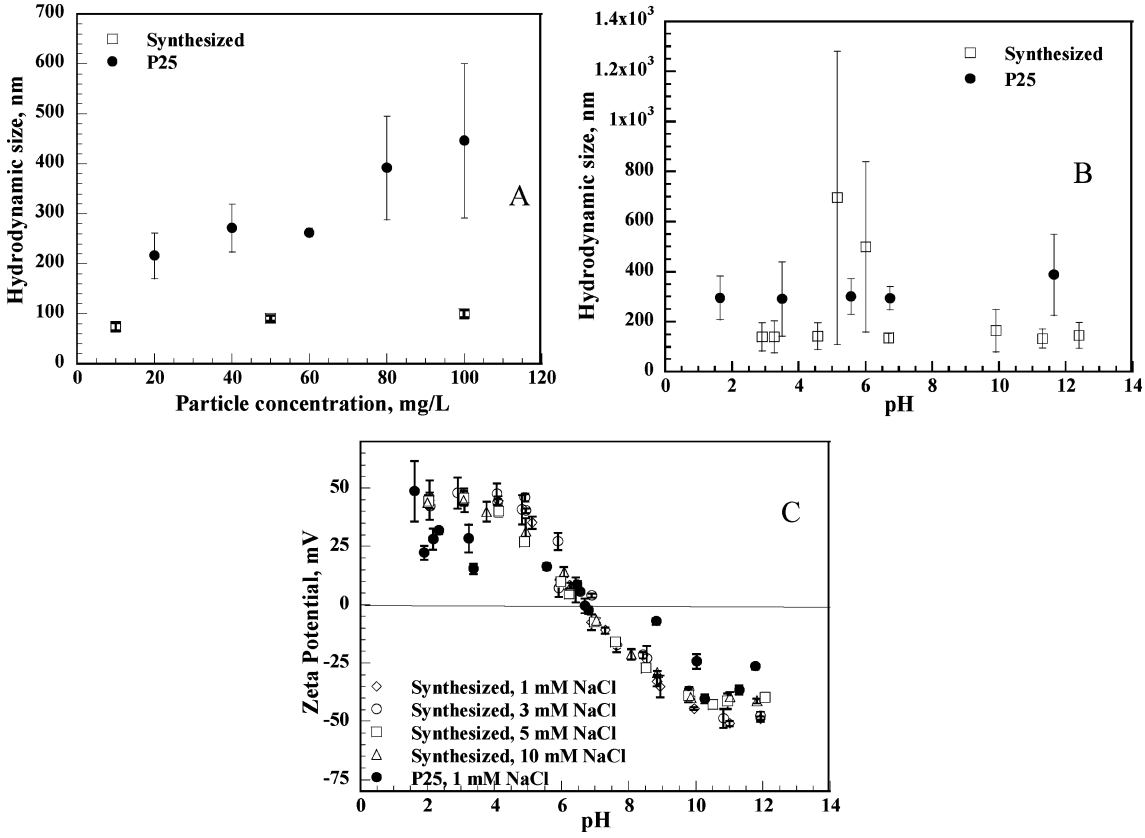

FIGURE 1. Characteristics of TiO_2: (A) hydrodynamic sizes as a function of concentration (error bars are ± 95% confidence intervals for three measurements) at pH 6.0 and 0 mM NaCl, (B) hydrodynamic sizes as a function of pH (error bars are ± one geometric standard deviation) for 30 mg/L NPs in 0.9 mM NaCl solutions, and (C) TiO_2 NP zeta potentials at different pHs.

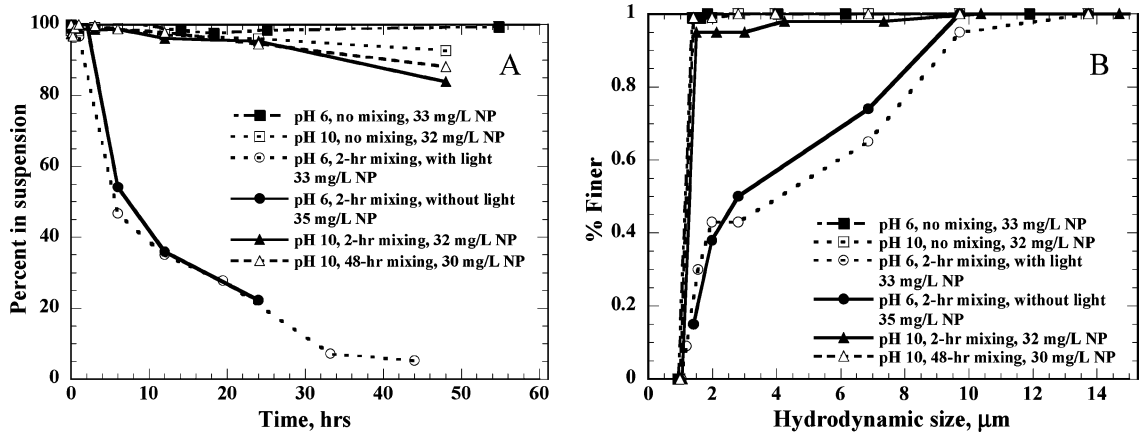

FIGURE 2. Batch experiment results for P25 TiO_2: (A) percent of NPs remaining in suspension over time, and (B) size distributions of NPs.

in-stream concentrations calculated using the 4-h and 72-h calibration equations. Thus, the measurement method used was not expected to cause significant errors in the results presented here.

Column Experiments. To obtain the filtration coefficient for the colloid exchange model, seven column experiments were conducted (see Table S1, SI). The column was a 25 mm i.d. glass chromatography column with adjustable endpieces (Omnifit, Cambridge, England). The same type of silica sand, NP preparation methods, and chemical conditions as used in the flume experiments were employed, following the method described in Ren et al. (*23*). Briefly, a minimum of 22 pore volumes of 0.9 mM NaCl solution were injected first using a Cole-Parmer Masterflex precision variable speed pump (Barnart Co. Barrington, IL) to estimate the effective porosity (n) of the packed column, followed by a minimum of 39 pore volumes of TiO_2 NP injection and a second injection of a minimum of 9 pore volumes of 0.9 mM NaCl to examine the NPs eluted from the column.

Batch Experiments. Batch experiments were conducted without mixing, with 2-h or 48-h slow mixing (75 r.p.m.) using a magnetic stirrer, and in the presence or absence of light to investigate the effect of sedimentation on NP exchange. The slow mixing mimics the flow condition in the flume system. After mixing, the suspensions from each batch were poured into a glass column with a height of 35.5 cm and an external diameter of 6 cm. The suspensions were allowed to settle, samples were taken over time from the

same height (8.8 cm), and their NP concentrations were determined.

Colloid Exchange Theory

Stream−subsurface exchange of colloidal particles induced by a dune-shaped bedform was modeled using advective pumping theory, colloid filtration, and settling by Packman et al. (*11*). In this model, pore water velocities of colloids in a finite streambed were calculated by considering advective pumping and particle settling (*11*):

$$u_{particle} = u = -kKh_m\cos(kx)[\tanh(kd_b)\sinh(ky) + \cosh(ky)] + u_u \quad (1a)$$

$$v_{particle} = -kKh_m\sin(kx)[\tanh(kd_b)\cosh(ky) + \sinh(ky)] - v_s\theta \quad (1b)$$

where $u_{particle}$ is the longitudinal Darcy velocity of colloids, $v_{particle}$ is the vertical Darcy velocity of colloids, K is the hydraulic conductivity of the streambed, h_m is the half amplitude of the head variation over the bedform, k is the bedform wavenumber ($k = 2\pi/\lambda$, λ is the dune wavelength), x is the longitudinal coordinate along the streambed, y is the vertical coordinate (perpendicular to x), d_b is the bed depth, $u_u = KS$ is the pore water flow due to the stream slope, S, v_s is the colloid settling velocity, and θ is the porosity of the streambed. Definitions of these variables are illustrated in Figure S1-B and more information can be found in refs *11* and *16*.

As colloids moved into the streambeds, the removal of colloids in porous media due to filtration was modeled using the classical filtration equation (*24*−*26*):

$$\frac{dC_c}{dL} = -\lambda_f C_c \quad (2)$$

where L is the distance traveled by colloids along flow paths through the bed, C_c is the mobile colloid concentration in the pore water, and λ_f is the colloid filtration coefficient.

The filtration coefficient is a function of both the physical transport and particle−particle interactions (*25*):

$$\lambda_f = \frac{3}{2}\frac{(1-\theta)}{d_c}\alpha_c\eta \quad (3)$$

where α_c is the clean-bed collision efficiency factor which represents all solution and particle surface chemistry effects, η is the single collector efficiency which represents all physical transport effect, and d_c is the average diameter of the collector grains of the porous medium. The single collector efficiency η, the fraction of incoming NPs that collide with the collector grains, was calculated using the TE equation described in ref *26*. To apply the colloid exchange model, a procedure similar to that used in ref *10* was employed to estimate the filtration coefficient from the column experiment results (see Text S2 in the SI).

Results

Characteristics of the Nanoparticles. The SEM micrograph of P25 TiO_2 dry powders showed that the P25 TiO_2 had a spherical shape and the nanoparticles were easily aggregated. The dry P25 TiO_2 had an aggregate size range of 100−250 nm (see Figure S2-a). TEM micrographs showed that both P25 TiO_2 and synthesized TiO_2 dry powder had a primary particle size of 20 nm (see Figure S2-b and -c). XRD results indicated that the synthesized TiO_2 NPs are amorphous and the P25 TiO_2 is composed of two crystalline phases including anatase (86.5%) and rutile (13.5%) (see Figure S3).

The hydrodynamic size of synthesized TiO_2 increased from 75 to 100 nm at pH 6.0 and 0 mM NaCl when the particle concentrations were increased from 10 to 100 mg/L (Figure 1A). For P25 TiO_2, even in the absence of potential destabilizing agents such as salts and organic material, the observed hydrodynamic size ranged from 216 to 446 nm for concentrations between 20 and 100 mg/L in DI water at pH 6.0. Thus, fresh P25 solutions were prepared prior to each experiment to minimize the effect caused by the spontaneous aggregation and the unstable behavior of aqueous P25 TiO_2 in this study.

The hydrodynamic sizes of synthesized TiO_2 ranged from 139 to 164 nm in the pH range of 2.9−12.4 in 0.9 mM NaCl solutions, except those tested at pHs 5.15 and 6, which were as high as 695 nm with very high geometric standard deviation (Figure 1B). The increased hydrodynamic size at pHs 5.15 and 6 is due to the weakened electrostatic repulsion between the NPs near the isoelectric point (Figure 1C) (*27*). The hydrodynamic sizes of P25 TiO_2 ranged from 296 to 387 nm for the pH range of 1.64−11.64, which were bigger than those observed for the synthesized TiO_2.

The zeta potentials for 10−30 mg/L NP suspensions at different NaCl concentrations are shown in Figure 1C. The isoelectrical point (the point of zero charge) was found to be 6.7 for P25 TiO_2 and 6.6 for synthesized TiO_2. This value agrees with previously reported values for TiO_2 (*28, 29*). Synthesized NPs show higher absolute values of surface charge at both high and low pHs than the P25 TiO_2, indicating higher electrostatic repulsive forces for the synthesized TiO_2 than the P25 TiO_2 at the same pHs (*30*). This might also contribute to the aforementioned smaller hydrodynamic sizes of the synthesized NPs compared to P25 NPs in the wide pH range tested. Variations in ionic strength (from 1 to 10 mM NaCl) did not significantly alter the surface charge of the synthesized TiO_2 NPs.

Batch Experiment Results. An ionic strength of 0.9 mM NaCl and NP concentrations of 30−35 mg/L were used in all batch experiments. Results indicated that without mixing, the changes in P25 TiO_2 concentration in the suspension were insignificant at pHs 6.0 and 10.0, indicating negligible sedimentation process and hydrodynamic size change between these two pHs (Figure 2A). This independence of hydrodynamic size on pH is consistent with the results shown in Figure 1B. Nevertheless, fast settling of the NPs occurred within the first a few hours for P25 TiO_2 at pH 6.0 after a 2-h mixing. White particle lumps were visible at the end of the 2-h mixing, suggesting that aggregation occurred during the slow mixing and resulted in increased particle size (Figure 2B). The critical coagulation concentration for 30 mg/L P25 TiO_2 suspension was found to be 0.8 mM NaCl at pH 6.0. At pH 10, the sedimentation, and thus the aggregation, induced by the 2- and 48-h slow mixing was insignificant. The aggregation and sedimentation were not affected by the presence of light. The synthesized TiO_2 NPs did not settle under the experimental conditions tested and they became unstable in 10 mM NaCl solution at pH 6.0.

Column Experiment Results. P25 and synthesized NPs reached their highest concentrations of $C/C_0 = 0.58$ and 0.95, respectively, at pH 6.0 (see Figure S4). At pH 9.6, almost all of the influent P25 TiO_2 appeared in the effluent at a column length of 2.7 cm. The α_c and λ_f values were calculated and are presented in Table S1. The average α_c values of column runs 1−3 were used in predicting results of flume run 1A for synthesized TiO_2 (Table 1). The average α_c values of column runs 4−6 were used in predicting results of flume run 2A for P25 TiO_2 (Table 1).

Flume Experiments. Dimensionless time (t^*/θ, where $t^*/\theta = k^2Kh_mt/\theta$) and in-stream concentrations (C/C_0, where C and C_0 are the NP concentrations at time t and t_0, respectively) were used to provide a comparison between flume runs with different pumping rates. The dimensionless time corresponds to the advective pumping mechanism; it is the time required

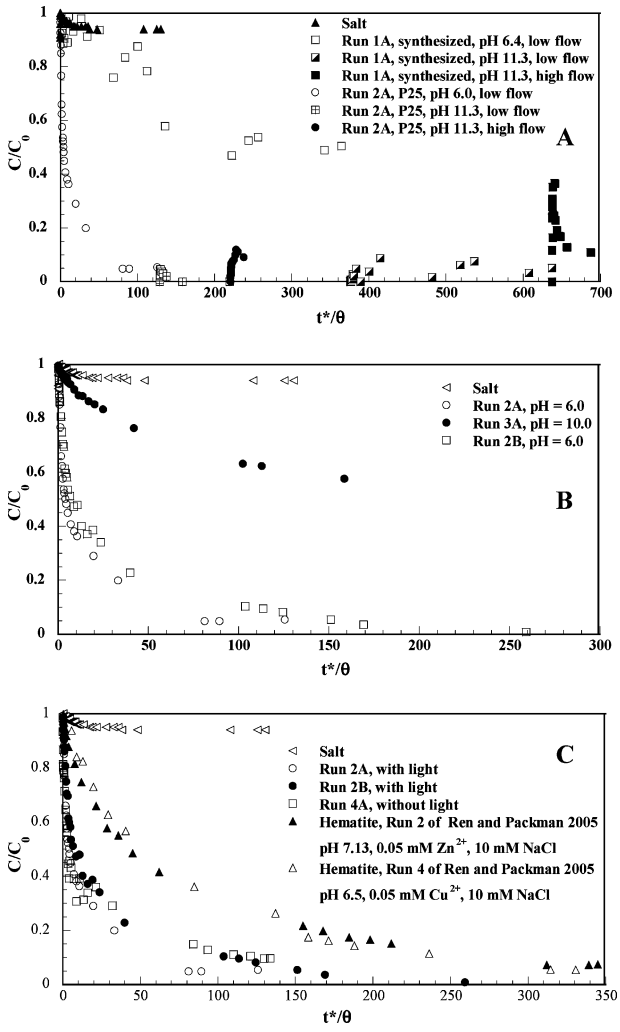

FIGURE 3. Comparisons of flume results: (A) synthesized TiO_2 vs P25 TiO_2. Note $t^*/\theta = 125$ corresponds to 24 h in Flume run 2A, (B) P25 TiO_2 at low and high pHs, and (C) effect of light on P25 TiO_2 exchange and their comparison with hematite colloids deposition. The hematite colloids were 100−200 nm in dry powder and 3.2 μm in liquid phase and the hydraulic conditions used in runs 2 and 4 of Ren and Packman (*15*) were similar to those used in this study.

for pore water to travel through the streambed at the characteristic seepage velocity $u_m/\theta = kKh_m/\theta$, where μ_m is the maximum Darcy velocity in the bed (*11*). At pH 6.0, the transport between the two types of NPs differed dramatically (Figure 3A). Both types of NPs had a positive surface charge, while the silica sand had a negative surface charge, presenting a favorable filtration condition in the streambed. As a result, deposition of both types of NPs was observed. The deposition of the P25 TiO_2 was at a much faster rate (almost all P25 TiO_2 NPs were deposited after 24 h, i.e., $t^*/\theta = 125$) compared with that of the synthesized TiO_2. The amount of synthesized TiO_2 that remained in the streamwater was significantly higher (about 50%) than the P25 TiO_2 NPs.

When the stream pH was above the isoelectrical point, a negative surface charge of the NPs and therefore an unfavorable filtration condition in the streambed was expected. Thus, when the pH was raised to 11.3, both types of nanoparticles were released (Figure 3A). The extent of this release, calculated as the difference of C/C_0 observed at high and low pHs, was 6−7% for the synthesized TiO_2 and 5% for the P25 TiO_2 NPs. The unstable data for the synthesized TiO_2 were attributed to measurement error. The release was further enhanced when the stream flow rates were doubled during the third phase experiment (Figure 3A). The increased flow rate caused deformation of the original bedforms and resuspension of both the sand and the previously deposited TiO_2 NPs. This release, calculated as the difference in C/C_0 in high and low flow conditions, was higher for the synthesized TiO_2 (∼37%) than the P25 TiO_2 (∼12%).

The deposition of the P25 TiO_2 NPs at different pHs is shown in Figure 3B. The results obtained from run 2B confirmed the fast deposition of the P25 NPs observed in run 2A. In run 3A, a stable in-stream concentration around 60% was observed, which was expected since the extent of aggregation and sedimentation at pH 10.0 was much less than that occurred at pH 6.0 (Figure 2).

To demonstrate the rapid deposition rate of the P25 TiO_2 caused by the aggregation and sedimentation, flume results of runs 2A and 2B were compared with the deposition of hematite obtained by Ren and Packman (*15*) in similar hydraulic conditions (Figure 3C). Despite the extremely high reactivity and decreased mobility of hematite due to the presence of metal ions (Zn^{2+} and Cu^{2+}), the deposition of P25 TiO_2 NPs was faster than the hematite colloids. Since no significant difference was found between results obtained from run 4A and those obtained from runs 2A and 2B, the presence of light was not contributing to the fast deposition of the P25 TiO_2 observed (Figure 3C).

Colloid Exchange Model Application. The exchange model reasonably predicted the deposition of the synthesized TiO_2 (Figure 4A). By assuming constant and uniform hydrodynamic sizes of NPs or their aggregates during the course of exchange, the model of Packman et al. was applied to simulate the deposition of the P25 TiO_2. Model simulation using the hydrodynamic sizes of 0.27 μm obtained from Figure 1A under-predicted the deposition of P25 TiO_2 NPs at pH 6.0 (Figure 4B). Considering possible errors originating during the filtration parameter estimation using column experiment results, model fitting was conducted by adjusting the filtration coefficient. It was found that a 10 times higher filtration coefficient did not result in any additional particle retention in the streambed. Thus, colloid filtration alone as a particle trapping mechanism is insufficient to describe the flume data (Figure 4B). When a hydrodynamic size of 2.8 μm obtained from Figure 2B was used, model simulation did show additional particle trapping, indicating the importance of particle settling in interpreting the observed flume data. However, to best describe the experimental data, a hydrodynamic size of 10.0 μm would be needed. This desired particle size increase is possible after considering the aggregation observed.

The model prediction for flume runs 3A and 3B was also above the experimental data (Figure 4C). After the filtration coefficient was increased from 0.023 cm^{-1} to 0.125 cm^{-1}, the model better simulated the deposition of the P25 TiO_2.

Discussion

Considerable aggregation was observed for P25 TiO_2 at pH 6.0 when slow mixing was applied, and it was not related to the presence of light. Such aggregation is not surprising for NPs, but is rare for large particles such as silica and clay under similar experimental conditions. The slow mixing process promoted interactions and contact of NPs, which led to particle aggregation. This flow-induced aggregation corresponds to the physical transport mechanisms described in the classical aggregation theory (*31*). It caused important sedimentation, which also dominated the exchange of P25 TiO_2.

The process-based colloid exchange model was applied to simulate the observed flume experiment data. The effect of increased hydrodynamic size due to aggregation was considered in the model simulation via the estimation of

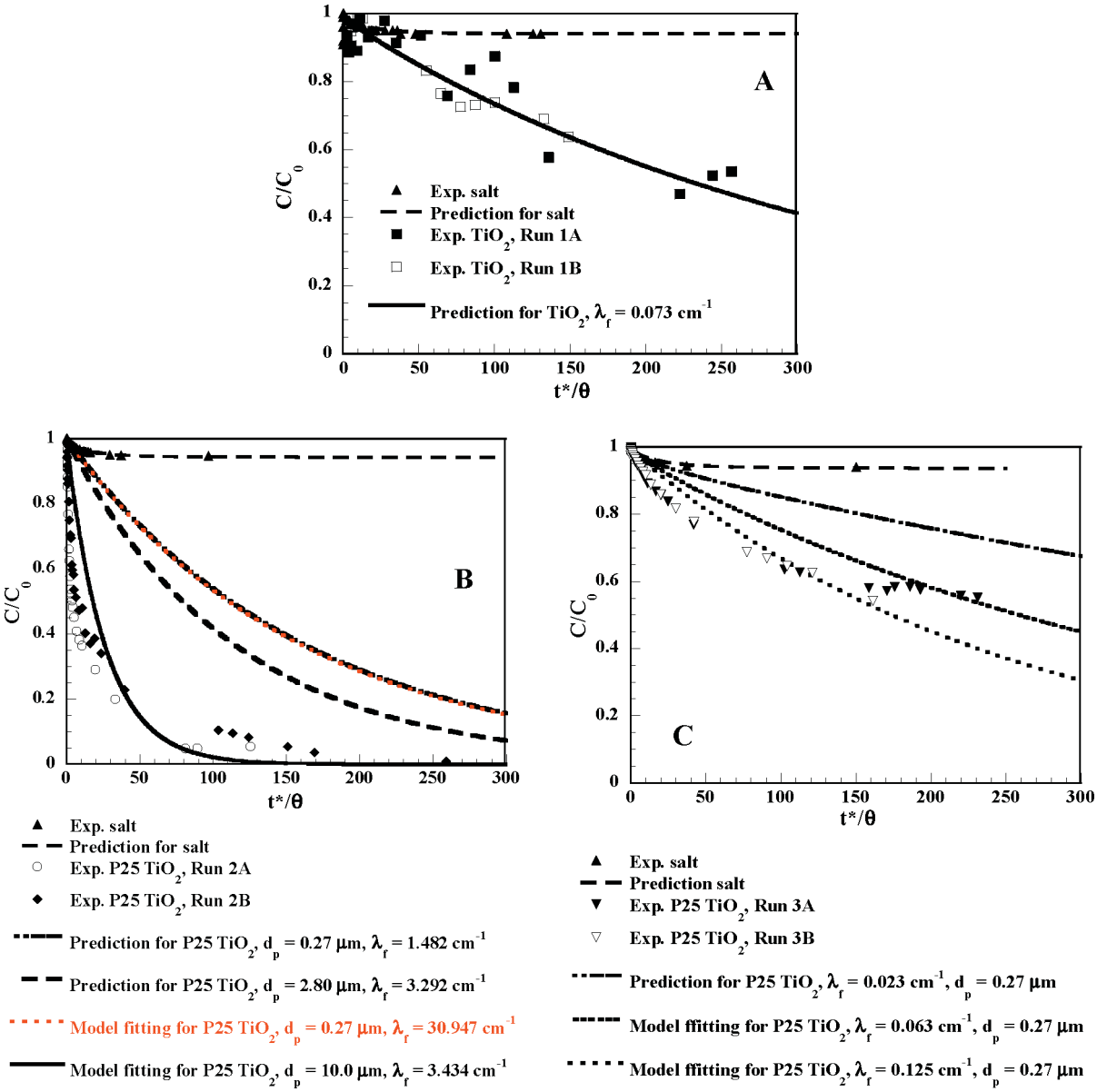

FIGURE 4. Exchange model applications: (A) synthesized TiO_2, (B) P25 TiO_2 for flume runs 2A and 2B, and (C) P25 TiO_2 for flume runs 3A and 3B.

filtration coefficient and particle settling velocity. The increased hydrodynamic size caused increased single collector efficiency and filtration coefficient, and therefore increased particle retention in the streambed. It also caused increased particle settling, which contributes to the early stage fast particle removal.

The deposition of synthesized TiO_2 was reasonably predicted using the colloid exchange model. However, significant discrepancy was found between the model predictions and the experimental data for P25 TiO_2. This large discrepancy can be explained using the colloid filtration theory for results obtained at pH 10.0, but not at pH 6.0. When the particle settling parameter was adjusted after considering the possible errors occurring in input parameter estimation, the model better fit the experimental data obtained at pH 6.0. Thus, the current process-based colloid exchange model simulated to some extent the deposition of P25 TiO_2. However, since the hydrodynamic size of the P25 TiO_2 NPs or their aggregates was assumed constant and uniform in the model simulation, errors caused by this assumption should not be neglected. Aggregation as an additional mechanism should be considered in detail in future studies to better analyze the observed processes during stream−subsurface exchange.

Release of both types of TiO_2 was observed due to the mobilization of these particles from the streambed through resuspension when the flow rate was increased. The P25 TiO_2 aggregates formed at pH 6.0 were easily broken. Particle disaggregation caused by increased fluid shear is documented in refs *30* and *32*. Thus, disaggregation might also contribute to the release of P25 TiO_2 NPs. Since the synthesized TiO_2 had more negative surface charge at pH 11.3 than the P25 TiO_2, thus higher electrostatic repulsive force which is favorable for particle disaggregation and detachment from silica sand, the synthesized TiO_2 had a higher release than the P25 TiO_2 at pH 11.3 when both particles were subjected to similar shear due to high flow rates.

The different behaviors for P25 TiO_2 NPs observed at pH 6.0 and 10.0 are attributed to the difference in their surface charges at these pHs. At pH 10.0, the surface of the P25 TiO_2 was more negative, which decreased the degree of aggregation and also made the deposition of P25 TiO_2 in the streambed less favorable. In addition, although the two types of TiO_2 had a similar zeta potential at pH 6.0, their deposition in the

streambed and the degree of aggregation were appreciably different at this pH. This difference might be attributed to the difference in their phase structure (crystalline vs amorphous) as also indicated by Murdock et al. (*5*). However, this hypothesis and the exact mechanism on how the phase structures might affect the deposition of the NPs will need further investigation in future studies.

Colloid filtration theory was also used by Choy et al. (*7*) in simulating TiO_2 NPs transport in sand columns. According to Stumm and Morgan (*31*), colloids are defined as particles having a size between 1 nm and 10 μm. Thus, the TiO_2 NPs tested can be viewed as colloids and the retention of TiO_2 NP in the sand column and streambed due to filtration can be assumed. The assumption that NPs behave like colloids can also be indirectly supported by the mobilization of the deposited TiO_2 NPs caused by increased flow as observed in flume runs 1A and 2A according to colloid mobilization theory (*30*). Also note that this release of the deposited TiO_2 NPs from streambed is very similar to what we observed for micrometer- and submicrometer-sized colloids such as kaolinite clay and hematite.

This work provided first-hand information on stream−subsurface exchange characteristics of TiO_2 NPs. Although only two types of TiO_2 NPs were tested, we anticipate that the results presented will lead to a broad range of further study on nanoparticle transport in natural streams. Since the two types of TiO_2 NPs demonstrated totally different transport behaviors, it will also be necessary to investigate other types of TiO_2 NPs synthesized using different techniques to draw generic conclusions relating to the fate and transport of manufactured nanomaterials.

Acknowledgments

This work was supported by the National Science Foundation CAREER award CBET-0449014 to J.R. We thank Jingbo L. Liu for her help on obtaining the phase structure of the nanoparticles using X-ray powder diffraction technique, and Roberto Candal for providing the synthesized TiO_2 nanoparticles. Thanks are also given to Linna Du and Jenny Curran, who helped with data collection.

Supporting Information Available

Text S1 describing the detailed procedure used to generate the synthesized TiO_2; Text S2 presenting the TE equation and method used to estimate the filtration coefficient for exchange model application; Table S1 describing the column experiment conditions and filtration parameters estimated; Figure S1 showing a picture of the flume; Figure S2 presenting the electron microscope images of the NPs; Figure S3 showing the phase structures of TiO_2 NPs; and Figure S4 presenting representative breakthrough curves of TiO_2 NPs through a sand column. This material is available free of charge via the Internet at http://pubs.acs.org.

Literature Cited

(1) Wiesner, M.; Bottero, J. Y. *Environmental Nanotechnology, Application and Impacts of Nanomaterials*; Mc Graw Hill: New York, 2007.

(2) Chen, X.; Mao, S. S. Titanium dioxide nanomaterials: synthesis, properties, modifications, and applications. *Chem. Rev.* **2007**, *107*, 2891–2959.

(3) Indris, S.; Amade, R.; Heitjans, P.; Finger, M.; Haeger, A.; Hesse, D.; Grunert, W.; Borger, A.; Becker, K. D. Preparation by high-energy milling, characterization, and catalytic properties of nanocrystalline TiO_2. *J. Phys. Chem. B* **2005**, *109*, 23274−23278.

(4) Klaine, S. J.; Alvarez, P. J. J.; Batley, G. E.; Fernandes, T. F.; Handy, R. D.; Lyon, D.; Mahendra, S.; McLaughlin, M. J.; Lead, J. R. Nanomaterials in the environment: behavior, fate, bioavailability, and effects. *Environ. Toxicol. Chem.* **2008**, *27* (9), 1825–1851.

(5) Murdock, R. C.; Braydich-Stolle, L.; Schrand, A. M.; Schlager, J. J.; Hussain, S. M. Characterization of nanomaterial dispersion in solution prior to in vitro exposure using dynamic light scattering technique. *Toxicol. Sci.* **2008**, *101* (2), 239–253.

(6) U.S. Environmental Protection Agency. *Nanotechnology White Paper*; 100/B-07/001; February 2007.

(7) Choy, C. C.; Wazne, M.; Meng, X. Application of an empirical transport model to simulate retention of nanocrystalline titanium dioxide in sand columns. *Chemosphere* **2008**, *71*, 1794–1801.

(8) Thibodeax, L. J.; Boyle, J. D. Bedform-generated convective transport in bottom sediment. *Nature* **1987**, *325* (22), 341–343.

(9) Harvey, J. W.; Bencala, K. E. The effect of streambed topography on surface-subsurface water exchange in mountain catchments. *Water Resour. Res.* **1993**, *29* (1), 89–98.

(10) Ren, J.; Packman, A. I. Effect of background water composition on stream-subsurface exchange of submicron colloids. *J. Environ. Eng.* **2002**, *128* (7), 624–634.

(11) Packman, A. I.; Brooks, N. H.; Morgan, J. J. A physicochemical model for colloid exchange between a stream and a sand streambed with bed forms. *Water Resour. Res.* **2000**, *36* (8), 2351–2361.

(12) Packman, A. I.; Brooks, N. H.; Morgan, J. J. Kaolinite exchange between a stream and streambed: laboratory experiments and validation of a colloid transport model. *Water Resour. Res.* **2000**, *36* (8), 2363–2372.

(13) Nagorski, S. A.; Moore, J. N. Arsenic mobilization in the hyporheic zone of a contaminated stream. *Water Resour. Res.* **1999**, *35* (11), 3441–3450.

(14) Fuller, C. C.; Harvey, J. W. Reactive uptake of trace metals in the hyporheic zone of a mining-contaminated stream, Pinal Creek, AZ. *Environ. Sci. Technol.* **2000**, *34*, 1150–1115.

(15) Ren, J.; Packman, A. I. Coupled stream-subsurface exchange of colloidal hematite and dissolved zinc, copper and phosphate. *Environ. Sci. Technol.* **2005**, *39*, 6387–6394.

(16) Elliott, A. H.; Brooks, N. H. Transfer of nonsorbing solutes to a streambed with bed forms: theory. *Water Resour. Res.* **1997**, *33* (1), 123–136.

(17) Elliott, A. H.; Brooks, N. H. Transfer of nonsorbing solutes to a streambed with bed forms: laboratory experiments. *Water Resour. Res.* **1997**, *33* (1), 137–151.

(18) Savant, S. A.; Reible, D. D.; Thibodeax, L. J. Convective transport within stable river sediments. *Water Resour. Res.* **1987**, *23* (9), 1763–1768.

(19) Bischoff, B.; Anderson, M. Peptization process in the sol-gel preparation of porous anatase (TiO_2). *Chem. Mater.* **1995**, *7*, 1772–1778.

(20) Ziemniak, S. E.; Jones, M. E.; Combs, K. E. S. Solubility behavior of titanium(IV) oxide in alkaline media at elevated temperatures. *J. Solution Chem.* **1993**, *22*, 601–623.

(21) Knauss, K. G.; Dibley, M. J.; Bourcier, W. L.; Shaw, H. F. Ti(IV) hydrolysis constants derived from rutile solubility measurements made from 100 to 300 °C. *Appl. Geochem.* **2001**, *16*, 1115–1128.

(22) Schmidt, J.; Vogelsberger, W. Dissolution kinetics of titanium dioxide nanoparticles: the observation of an unusual kinetic size effect. *J. Phys. Chem. B* **2006**, *110*, 3955–3963.

(23) Ren, J.; Packman, A. I.; Welty, C. Correlation of colloid collision efficiency with hydraulic conductivity of silica sands. *Water Resour. Res.* **2000**, *36* (9), 2493–2500.

(24) Iwasaki, T. Some notes on sand filtration. *J. Am. Water Works Assoc.* **1937**, *29*, 1591–1597.

(25) Yao, K. M.; Habibian, M. T.; O'Melia, C. R. Water and waste water filtration: concepts and applications. *Environ. Sci. Technol.* **1971**, *5* (11), 1105–1112.

(26) Tufenkji, N.; Elimelech, M. Correlation equation for predicting single-collector efficiency in physicochemical filtration in saturated porous media. *Environ. Sci. Technol.* **2004**, *38*, 529–536.

(27) Jiang, J.; Oberdorster, G.; Biswas, P. Characterization of size, surface charge, and agglomeration state of nanoparticle dispersions for toxicological studies. *J. Nanopart. Res.* **2008**; DOI 10.1007/s11051-008-9446-4.

(28) Lyklema, J. *Fundamentals of Interface and Colloid Science*; Academic Press: London, 1995; Vol. II, A3.3.

(29) Kosmulski, M. The pH-dependent surface charging and the points of zero charge. *J. Colloid Interface Sci.* **2002**, *253*, 77–87.

(30) Ryan, J. N.; Elimelech, M. Colloid mobilization and transport in groundwater. *Colloids Surf. A* **1996**, *107*, 1–56.

(31) Stumm, W.; Morgan, J. J. *Aquatic Chemistry: Chemical Equilibria and Rates in Natural Waters*; John Wiley: New York, 1996.

(32) Newman, K. A.; Stolzenbach, K. D. Kinetics of aggregation and disaggregation of titanium dioxide particles and glass beads in a sheared fluid suspension. *Colloids Surf. A* **1996**, *107*, 189–203.

ES900424N